PHOTONIC SENSORS / Vol. 7, No. 4, 2017: 336–344

HCPCF-Based In-Line Fiber Fabry-Perot Refractometer and High Sensitivity Signal Processing Method

Xiaohui LIU, Mingshun JIANG*, Qingmei SUI, Xiangyi GENG, and Furong SONG

School of Control Science and Engineering, Shandong University, Jinan, 250061, China

*Corresponding author: Mingshun JIANG E-mail: jiangmingshun@sdu.edu.cn

Abstract: An in-line fiber Fabry-Perot interferometer (FPI) based on the hollow-core photonic crystal fiber (HCPCF) for refractive index (RI) measurement is proposed in this paper. The FPI is formed by splicing both ends of a short section of the HCPCF to single mode fibers (SMFs) and cleaving the SMF pigtail to a proper length. The RI response of the sensor is analyzed theoretically and demonstrated experimentally. The results show that the FPI sensor has linear response to external RI and good repeatability. The sensitivity calculated from the maximum fringe contrast is –136 dB/RIU. A new spectrum differential integration (SDI) method for signal processing is also presented in this study. In this method, the RI is obtained from the integrated intensity of the absolute difference between the interference spectrum and its smoothed spectrum. The results show that the sensitivity obtained from the integrated intensity is about -1.34×10^5 dB/RIU. Compared with the maximum fringe contrast method, the new SDI method can provide the higher sensitivity, better linearity, improved reliability, and accuracy, and it's also convenient for automatic and fast signal processing in real-time monitoring of RI.

Keywords: Optical fiber sensor; in-line Fabry-Perot interferometer; hollow-core photonic crystal fiber; refractive index; spectrum differential integration method

Citation: Xiaohui LIU, Mingshun JIANG, Qingmei SUI, Xiangyi GENG, and Furong SONG, "HCPCF-Based In-Line Fiber Fabry-Perot Refractometer and High Sensitivity Signal Processing Method," *Photonic Sensors*, 2017, 7(4): 336–344.

1. Introduction

Refractive index (RI) measurement of liquids has great significance in chemistry, biology, industry, food processing, and environmental monitoring, etc. Optical fiber refractometers have attracted widespread attention in the past decades due to many desirable advantages such as the small size, compact structure, high flexibility, immunity to electromagnetic interference, corrosion resistance, and the capacity for *in situ* and multiplexed operation. Various optical fiber refractometers have been developed including tapered fiber structures [1], optical fiber surface plasmon resonance (SPR) devices [2–3], fiber Bragg gratings (FBGs) [4–5], titled fiber Bragg gratings (TFBGs) [6], long-period gratings (LPGs) [7–8], optical fiber modal interferometers (MIs) [9–10], and fiber Fabry-Perot interferometers (FPIs) [11–16]. Among them, the fiber FPIs have advantages of compact probe structure, large measurement range, linear response, low temperature cross-sensitivity, and convenient reflection mode for detection, which make them particularly attractive for RI measurement.

Generally, the fiber FPIs can be classified into three types: extrinsic, intrinsic, and the recently

Received: 29 November 2016 / Revised: 10 February 2017

DOI: 10.1007/s13320-017-0392-6
Article type: Regular

developed in-line fiber FPIs. The extrinsic fiber FPI usually has an external cavity formed by two aligned fiber end faces [11]. And RI sensing can be realized by demodulating the optical path difference (OPD) when the analyte enters the cavity. Many signal processing methods have been presented for OPD demodulation such as peak wavelength tracing [17], peak-to-peak method [18], and fast Fourier transform (FFT) [19]. The extrinsic fiber FPI can provide a relatively high sensitivity. However, the open cavity is easily contaminated, which also suffers from structural instability and high optical transmission loss. The intrinsic fiber FPI is typically formed by two in-fiber mirrors [12]. The RI variation of the analyte will change the reflectivity of the exposed fiber end face, leading to a change in the interference fringe contrast. Normally, the intrinsic fiber FPI is difficult to be fabricated and has a relatively low fringe contrast. The in-line fiber FPI has a hybrid structure combining the characteristics of extrinsic and intrinsic FPIs [13–16]. It has been a hotspot in recent years due to its good performance and easy fabrication.

The RI measuring principle of the in-line fiber FPI is the same as the intrinsic FPI, and the RI of the analyte is usually obtained from the maximum fringe contrast of the interference spectrum [13, 14]. However, it requires a high signal-to-noise ratio (SNR) to calculate the maximum fringe contrast accurately. D. Wu *et al.* [15] used the FFT algorithm to obtain the spatial frequency spectrum of interference fringe and determined the RI by the peak amplitude, but a limitation of FFT is its poor resolution. They also proposed a spectrum differential integration (SDI) method [16] to calculate the RI induced intensity change of the interference spectrum. This method can improve the reliability and sensitivity for RI measurement; however, it needs one basic spectrum for every subtraction. So a more accurate, reliable, convenient, and high sensitive signal processing method is needed for the in-line fiber FPI refractometer.

In this paper, we propose an in-line fiber FPI refractometer based on the hollow-core photonic crystal fiber (HCPCF). The FPI is formed by splicing the both ends of a short section of the HCPCF to single mode fibers (SMFs) and cleaving the SMF pigtail to a proper length. The RI response of the FPI sensor is analyzed theoretically and demonstrated experimentally. Owing to its compact structure, good performance, simple and safe fabrication and so on, the proposed in-line fiber FPI refractometer shows a great promise for RI measurement. And a new signal processing method based on SDI is proposed in this study. The smoothed spectrum is used for subtraction instead of the basic spectrum. Experimental results show that compared with the maximum fringe contrast method, the new SDI method can provide higher sensitivity, better linearity, and improved reliability and accuracy. Besides, it's also convenient for automatic and fast signal processing in real-time monitoring of RI.

2. Theory

2.1 RI detection principle

The structure of the proposed in-line fiber FPI refractometer is shown in Fig. 1. A short section of the HCPCF is performed as an in-fiber air cavity. One end of the HCPCF is spliced to the SMF, and the other end is spliced to another short section of the SMF. The core RI of the SMF ($n_{\mathrm{SMF}} \approx 1.457$) is different from the HCPCF ($n_{\mathrm{HCPCF}} \approx 1$), thus three reflecting surfaces denoted as M1, M2, and M3 are formed due to Fresnel reflection. There are three Fabry-Perot cavities in this structure: Cavity 1 formed by M1 and M2 with a length L_1, Cavity 2 formed by M2 and M3 with a length L_2, and the longest Cavity 3 formed by M1 and M3 with a length equal to L_1+L_2.

The intensity reflectivities of the three surfaces are R_1, R_2, and R_3, respectively, which can be

calculated as follows according to the Fresnel reflection equation at normal incidence:

$$R_1 = R_2 = \left[\frac{n_{\mathrm{SMF}} - n_{\mathrm{HCPCF}}}{n_{\mathrm{SMF}} + n_{\mathrm{HCPCF}}}\right]^2, R_3 = \left[\frac{n_{\mathrm{SMF}} - n_{\mathrm{EX}}}{n_{\mathrm{SMF}} + n_{\mathrm{EX}}}\right]^2 \quad (1)$$

where n_{SMF} is the core RI of the SMF, n_{HCPCH} is the core RI of the HCPCF, and n_{EX} is the RI of the external medium (the analyte). Due to the significant RI difference between the HCPCF and SMF and the low light transmission loss of the HCPCF, the optical fiber FPI based on the HCPCF can provide the relatively high reflectivity and signal-to-noise ratio (SNR).

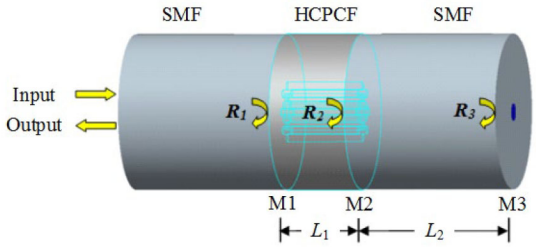

Fig. 1 Structure of the proposed FPI based on HCPCF.

Assume the electric field of the incident light is E_0. The light propagates along the fiber and is reflected by three surfaces, respectively. Notice that there is a π phase shift at the surface when light is reflected from an optically denser medium. Thus the combined reflected electric field E_r can be written as

$$E_r = E_0\sqrt{R_1} + E_0(1-R_1)(1-\alpha_1)(1-\gamma_1)\sqrt{R_2}\,\mathrm{e}^{\mathrm{i}(\phi_1+\pi)} + E_0(1-\alpha_1)(1-\alpha_2)(1-\gamma_1)(1-\gamma_2)(1-R_1)(1-R_2)\sqrt{R_3}\,\mathrm{e}^{\mathrm{i}(\phi_1+\phi_2)} \quad (2)$$

where α_1 and α_2 are the intensity attenuation factors due to the mode mismatch and surface imperfection of M1 and M2, respectively; γ_1 and γ_2 are defined as the optical transmission loss factors of the FP Cavity 1 and Cavity 2, respectively; ϕ_1 and ϕ_2 are the light phase delays (round-trip) induced by Cavity 1 and Cavity 2, and can be expressed as

$$\phi_1 = \frac{4\pi n_{\mathrm{HCPCF}} L_1}{\lambda}, \ \phi_2 = \frac{4\pi n_{\mathrm{SMF}} L_2}{\lambda} \quad (3)$$

where L_1 and L_2 are the lengths of Cavity 1 and Cavity 2, respectively, and λ is the wavelength of incident light.

The normalized intensity reflectivity R_{FP} of the FPI can be calculated by the following equation:

$$R_{\mathrm{FP}} = \frac{E_r \cdot E_r^*}{E_0^2}. \quad (4)$$

According to (1), (2), and (4), the RI of the external medium n_{EX} will affect the output R_{FP} through the intensity reflectivity R_3. Figure 2 shows the simulated interference spectra (R_{FP} & λ) of the proposed FPI with different n_{EX}. The simulated parameters are: $n_{\mathrm{SMF}} = 1.457$, $n_{\mathrm{HCPCH}} = 1$, $L_1 = 20\,\mu\mathrm{m}$, $L_2 = 775\,\mu\mathrm{m}$, $\alpha_1 = \alpha_2 = 0.15$, $\gamma_1 = 0.02$, and $\gamma_2 = 0.01$. λ is from 1 510 nm to 1 590 nm, and $n_{\mathrm{EX}} = 1$ (air), 1.33 (water), 1.38, and 1.44, respectively.

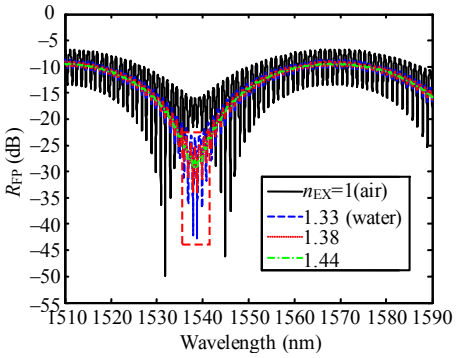

(a)

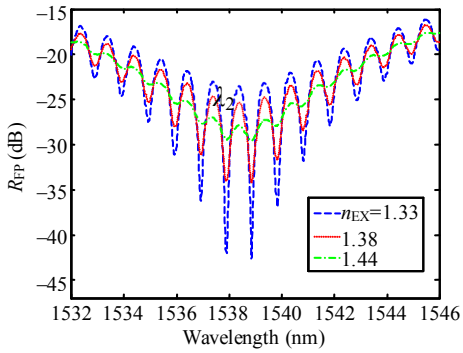

(b)

Fig. 2 Simulated interference spectra: (a) $n_{\mathrm{EX}} = 1$, 1.33, 1.38, and 1.44, respectively (other simulated parameters are: $n_{\mathrm{SMF}} = 1.457$, $n_{\mathrm{HCPCF}} = 1$, $L_1 = 20\,\mu\mathrm{m}$, $L_2 = 775\,\mu\mathrm{m}$, $\alpha_1 = \alpha_2 = 0.15$, $\gamma_1 = 0.02$, $\gamma_2 = 0.01$, and λ is from 1 510 nm to 1 590 nm) and (b) close-up of the spectra in liquids of different RIs.

As shown in Fig. 2, the fringe contrast of the interference spectrum changes when n_{EX} changes, so

the RI of the analyte can be determined by measuring the fringe contrast. Usually, the interference fringe that gives the maximum fringe contrast is chosen to obtain a better sensitivity [13]. By locating the absolute minimum $R_{FP}(\lambda_1)$ and the adjacent peak $R_{FP}(\lambda_2)$ as shown in Fig. 2(b), the maximum fringe contrast can be calculated by $V_{max} = \left|10\lg[R_{FP}(\lambda_2)/R_{FP}(\lambda_1)]\right|$ and in a logarithmic scale $V_{max} = \left|R_{FP}(\lambda_2) - R_{FP}(\lambda_1)\right|$ (unit: dB). V_{max} is completely free from the influences of light source intensity variation and transmission loss change. It is the most commonly used method for the in-line fiber FPI refractometer. However, it requires a high SNR to locate the trough and adjacent peak in the spectrum and readout their intensities accurately. Especially, when the external RI increases, the fringe contrast and SNR will decrease, causing large errors.

2.2 New SDI method

The SDI method [10] is essentially an intensity measurement method proposed by Y. Li *et al.*, and D. Wu *et al.* [16] used it to analyze the interference spectra of the FPI. They chose the spectrum obtained by putting the sensor in deionized water as the basic spectrum for every subtraction. However, the wavelength shift of the interference spectrum caused by ambient temperature variation [20] will bring errors for RI measurement.

So here we propose to use the smoothed spectrum instead of the basic spectrum for subtraction. As we can see in Fig. 2, the interference spectrum becomes more smoothed with an increase in RI. Thus in the new SDI method, first for each collected spectrum, a smoothed spectrum is obtained by smoothing function. Then the absolute intensity difference between the interference spectrum and its smoothed spectrum is calculated by pointwise subtraction at each wavelength. And at last, the absolute differences are integrated along the scanning wavelength range of the spectrum. The integrated intensity can be expressed as

$$I_{integrate} = \sum_{\lambda_0}^{\lambda_0 + N\cdot\Delta\lambda} \left|I(\lambda) - I_{smooth}(\lambda)\right| \cdot \frac{\Delta\lambda}{RBW} \tag{5}$$

where $I(\lambda)$ is the intensity of the recorded interference spectrum, $I_{smooth}(\lambda)$ is the smoothed spectrum, λ_0 is the starting wavelength, N is the number of data points collected in actual measurement, $\Delta\lambda$ is the interval between adjacent data, and RBW is the resolution bandwidth of the interrogator. Compared with the maximum fringe contrast method, the new SDI method can provide the higher sensitivity and improved reliability and accuracy, since more spectral information is included in demodulating the final result.

3. Experiment

3.1 Sensor fabrication

To fabricate the proposed FPI, one end of the HCPCF was cleaved and spliced to the SMF using a commercial electric arc fusion splicer (KL-280G) by manual operation. Then the other end of the HCPCF was cleaved to a desirable length and spliced to another section of the SMF. Finally, the subsequent SMF was cleaved to a suitable length. The cross-section of the HCPCF (HC19-1550, NKT Photonics) used in the experiment is shown in the inset of Fig. 3(a). It guided light in the central hollow core surrounded by a micro-structured cladding formed by a periodic arrangement of air holes in silica. The core diameter and the outer cladding diameter of HC19-1550 were ~20 μm and ~115 μm, respectively, and its mode field diameter was ~13 μm.

To minimize the air hole collapse of the HCPCF near splicing joint, we chose a weaker fusion power and a shorter fusion time, and introduced a suitable offset between the joint and the central axis of arc discharge to ensure a smaller amount of heat being applied to the HCPCF. The optimal splicing parameters in our fabrication process were: pre-fusion power of 10 bit, pre-fusion time of 150 ms,

arc fusion power of 30 bit, arc duration of 300 ms, overlap of 15 μm, and offset length of 15 μm. The microscopic image of the fabricated FPI is shown in Fig. 3(a). We can see that the air hole collapse of the HCPCF is avoided. The lengths of the HCPCF and the pigtail SMF were about 20.8 μm and 775 μm, respectively. The whole fabrication process was cost-effective and simple since only ordinary tools were needed.

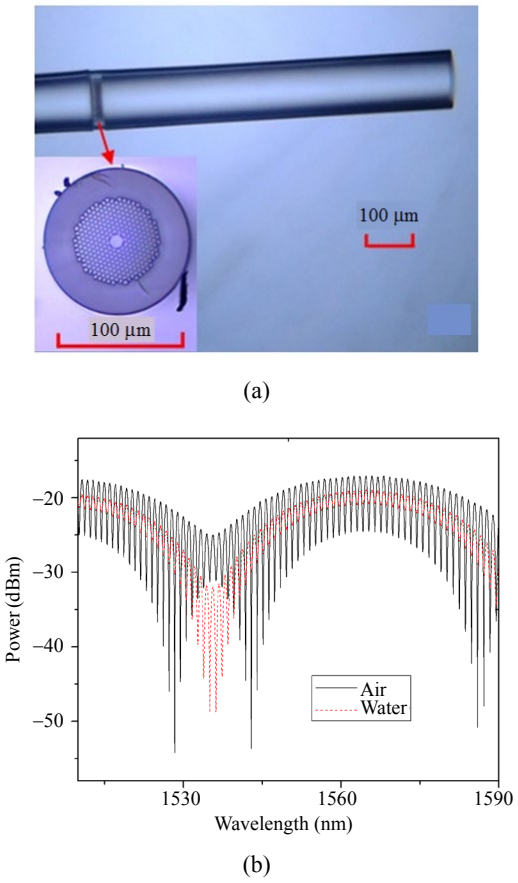

Fig. 3 Experimental results of sensor fabrication: (a) microscopic images of the fabricated FPI and the cross-section of HC19-1550 (inset) and (b) interference spectra of the fabricated FPI in air and water.

The reflective interference spectra of the fabricated FPI in air (n_{EX}=1) and water (n_{EX}=1.33) measured by an interrogator (SM125, Micron Optic Inc) are shown in Fig. 3(b). We can see that the FPI has a good fringe visibility (maximum fringe contrast ~17 dB in water) due to the relatively high RI difference between the HCPCF and SMF, and the low-loss high-quality splice.

3.2 RI measurement

Sucrose solutions with different concentrations (0 – 60%, corresponding RI: 1.33 RIU – 1.44 RIU, calibrated by an ABBE refractometer) were prepared to investigate the RI response of the FPI refractometer. The experimental setup is shown in Fig. 4. The fabricated FPI was dipped into the sucrose solutions vertically, and the reflected spectra were measured by SM125. A computer was used to record and process the signal. The sensor was cleaned by distilled water and dried water before the next test. The experiment was carried out at room temperature (25 ℃). The test was repeated for 3 times to investigate the repeatability.

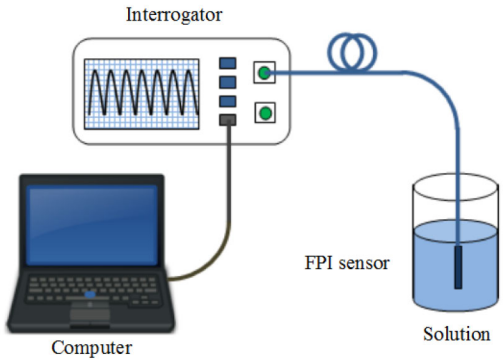

Fig. 4 Experimental setup for RI measurement.

4. Results and discussion

4.1 RI response

The reflective interference spectra of the FPI sensor in different solutions are shown in Fig. 5. It can be seen that the fringe contrast of the interference spectrum decreases as the external RI increases, which is consistent with the theory. The minor shift of the fringe wavelength may be caused by the ambient temperature variations. Figure 6 shows the relationship between the maximum fringe contrast V_{max} and external RI obtained from three tests. We can see that V_{max} decreases monotonically with an increase in RI in the range of 1.33 RIU – 1.44 RIU (refractive index unit). The FPI sensor

shows the linear response and good repeatability. The R-square value of linear fitting (average of three tests) is about 98%. The sensitivity obtained by V_{max} is –136 dB/RIU. With the intensity resolution of 0.01 dB for SM125, the RI resolution of the FPI sensor is about 7×10^{-5} RIU.

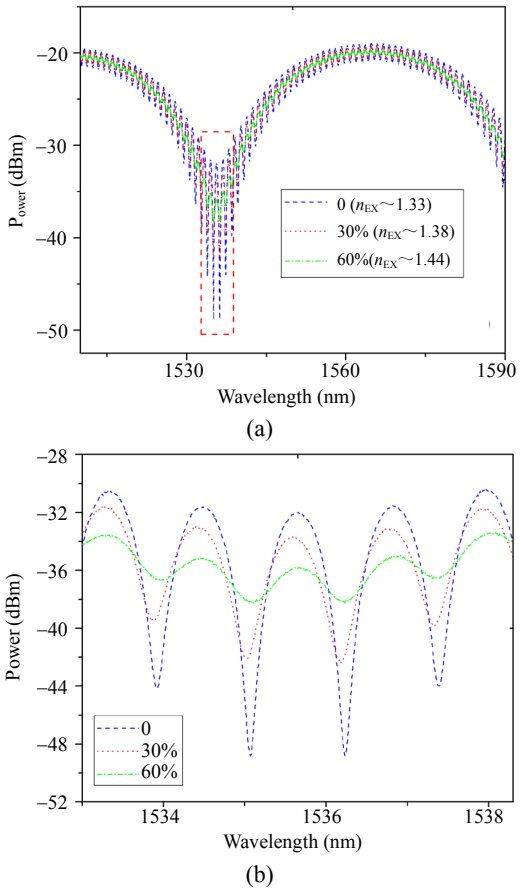

Fig. 5 Experimental results: (a) interference spectra of the FPI in solutions with different concentrations corresponding to different RI (0, 30% and 60%) and (b) close-up display.

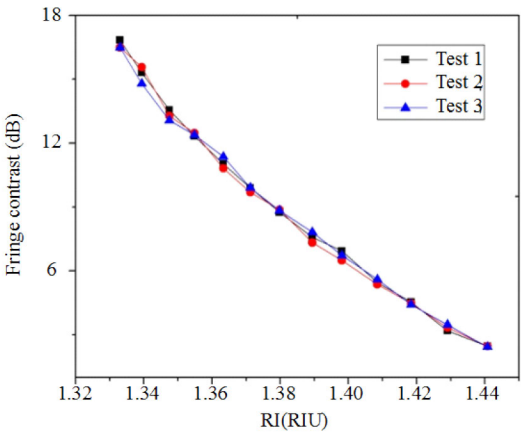

Fig. 6 Relationship between the maximum fringe contrast (V_{max}) and external RI for three tests.

Compared with our previous work [21], the sensor performance is enhanced, and the RI sensitivity is almost two times larger than the previous one. This is mainly due to the improvement of the sensor's fabrication quality.

4.2 New SDI method

The experimental results obtained by new SDI signal processing methods are shown in Figs. 7 and 8. In the proposed new SDI method, a smoothing function is applied to each acquired interference spectrum, and the smoothing function adopted in our experiment is the Savitzky-Golay method [22]. It's a widely used smoothing algorithm based on local polynomial fitting using the least square method. The smoothed spectra (dotted line) for different external RIs are shown in Fig. 7. Proper parameters for Savitzky-Golay method such as points of window and polynomial order are selected to fit the envelope of the interference spectrum better. Then the absolute intensity difference between the interference spectrum and its smoothed spectrum is calculated by pointwise subtraction at each wavelength. And the absolute differences are integrated along the scanning wavelength range of the spectrum. For the signal processing in our experiments, the scanning range is from 1 510 nm to 1 590 nm, the intervals between adjacent data and *RBW* of SM125 are both 5 pm.

The relationship between the integrated intensity $I_{integrate}$ and external RI is shown in Fig. 8. It can be seen that $I_{integrate}$ shows the same varying trend as V_{max}, but with an obviously improved linearity and accuracy. The R-square value of linear fitting (average of the three tests) is about 99.8%. The results obtained by the new SDI method are more reliable because the whole spectral information is included in calculation. The sensitivity obtained by $I_{integrate}$ is about -1.34×10^{5} dB/RIU, which is greatly improved. The sensitivity is found to be related to the scanning wavelength range and resolution of the

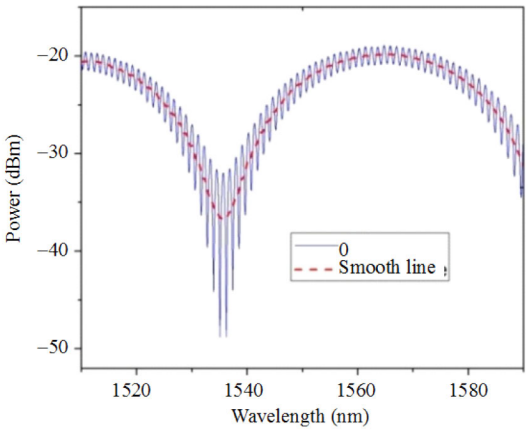

(a)

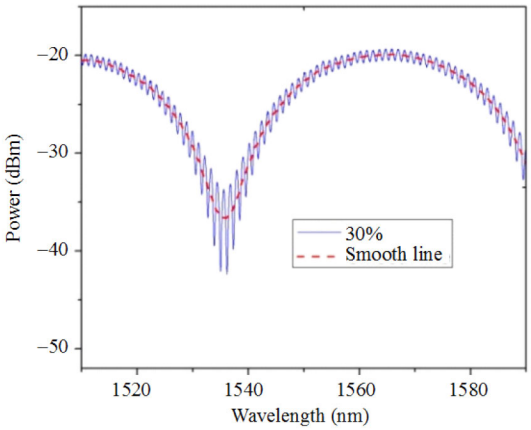

(b)

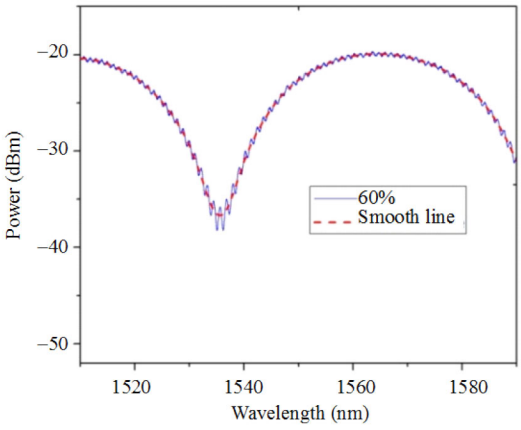

(c)

Fig. 7 Interference spectra (solid line) and smoothed spectra (dashed line) of the FPI in solutions of different concentrations corresponding to different RI: (a) 0, (b) 30%, and (c) 60%.

interrogator [10]. A wider scanning range and a higher resolution can result in a higher sensitivity, because more data points are added to the integral result. In a word, compared with the maximum fringe contrast method, the new SDI method can provide the higher sensitivity, better linearity, and improved reliability and accuracy.

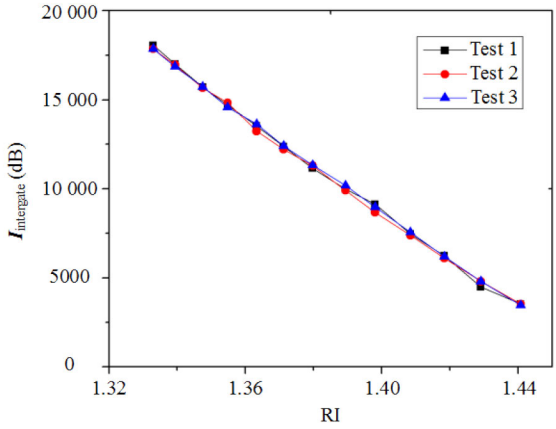

Fig. 8 Relationship between the integrated intensity ($I_{integrate}$) and external RI for three tests.

5. Conclusions

An in-line fiber FPI refractometer based on the HCPCF has been proposed in this paper. The RI response of the sensor is analyzed theoretically and demonstrated experimentally. Results show that the FPI sensor has the linear response to the external RI and good repeatability. The sensitivity calculated by the maximum fringe contrast is –136 dB/RIU. And a new signal processing method based on the SDI has also been presented in this study. In this new SDI method, the RI is obtained by the integrated intensity of the absolute difference between the interference spectrum and its smoothed spectrum. The signal processing results show that the sensitivity obtained by the integrated intensity is about -1.34×10^5 dB/RIU. Compared with the maximum fringe contrast method, the new SDI method can provide higher sensitivity, better linearity, and improved reliability and accuracy. And it's also convenient for automatic and fast signal processing in real-time monitoring of RI.

Acknowledgment

This research is supported by the National Natural Science Foundations of China (Grant Nos. 61174018 and 61505097) and Fundamental research funds of Shandong University, China (Grant No.

2014YQ009).

References

[1] D. J. Feng, G. X. Liu, X. L. Liu, M. S. Jiang, and Q. M. Sui, "Refractive index sensor based on plastic optical fiber with tapered structure," *Applied Optics*, 2014, 53(10): 2007–2011.

[2] J. Zhao, S. Q. Cao, C. R. Liao, Y. Wang, G. J. Wang, X. Z. Xu, *et al.*, "Surface plasmon resonance refractive sensor based on silver-coated side-polished fiber," *Sensors and Actuators B: Chemical*, 2016, 230: 206–211.

[3] S. Singh, S. K. Mishra, and B. D. Gupta, "Sensitivity enhancement of a surface plasmon resonance based fibre optic refractive index sensor utilizing an additional layer of oxides," *Sensors and Actuators A: Physical*, 2013, 193: 136–140.

[4] G. Tsigaridas, D. Polyzos, A. Ioannou, M. Fakis, and P. Persephonis, "Theoretical and experimental study of refractive index sensors based on etched fiber Bragg gratings," *Sensors and Actuators A: Physical*, 2014, 209: 9–15.

[5] Y. Ran, L. Jin, L. P. Sun, J. Li, and B. O. Guan, "Temperature-compensated refractive-index sensing using a single Bragg grating in an abrupt fiber taper," *IEEE Photonics Journal*, 2013, 5(2): 7100208–7100208.

[6] B. Q. Jiang, X. Lu, X. T. Gan, M. Qi, Y. D. Wang, L. Han, *et al.*, "Graphene-coated tilted fiber-Bragg grating for enhanced sensing in low-refractive-index region," *Optics Letters*, 2015, 40(17): 3994–3997.

[7] A. Singh, "Long period fiber grating based refractive index sensor with enhanced sensitivity using Michelson interferometric arrangement," *Photonic Sensors*, 2015, 5(2): 172–179.

[8] L. Coelho, D. Viegas, J. L. Santos, and J. M. M. M. de Almeida, "Enhanced refractive index sensing characteristics of optical fibre long period grating coated with titanium dioxide thin films," *Sensors and Actuators B: Chemical*, 2014, 202: 929–934.

[9] Y. Li, Z. B. Liu, and S. S. Jian, "Multimode interference refractive index sensor based on coreless fiber," *Photonic Sensors*, 2014, 4(1): 21–27.

[10] Y. Li, E. Harris, L. Chen, and X. Y. Bao, "Application of spectrum differential integration method in an in-line fiber Mach-Zehnder refractive index sensor," *Optics Express*, 2010, 18(8): 8135–8143.

[11] R. Gao, Y. Jiang, W. H. Ding, Z. Wang, and D. Liu, "Filmed extrinsic Fabry-Perot interferometric sensors for the measurement of arbitrary refractive index of liquid," *Sensors and Actuators B: Chemical*, 2013, 177: 924–928.

[12] C. L. Lee, J. M. Hsu, J. S. Horng, W. Y. Sung, and C. M. Li, "Microcavity fiber Fabry-Pérot interferometer with an embedded golden thin film," *IEEE Photonics Technology Letters*, 2013, 25(9): 833–836.

[13] Z. L. Ran, Y. J. Rao, W. J. Liu, X. Liao, and K. S. Chiang, "Laser-micromachined Fabry-Perot optical fiber tip sensor for high-resolution temperature-independent measurement of refractive index," *Optics Express*, 2008, 16(3): 2252–2263.

[14] Y. Gong, Y. Guo, Y. J. Rao, T. Zhao, and Y. Wu, "Fiber-optic Fabry-Perot sensor based on periodic focusing effect of graded-index multimode fibers," *IEEE Photonics Technology Letters*, 2010, 22(23): 1708–1710.

[15] D. Wu, Y. Huang, J. Y. Fu, and G. Y. Wang, "Fiber Fabry-Perot tip sensor based on multimode photonic crystal fiber," *Optics Communications*, 2015, 338: 288–291.

[16] D. Wu, W. Huang, G. Y. Wang, J. Y. Fu, and Y. Y. Chen, "In-line fiber Fabry-Perot refractive index tip sensor based on photonic crystal fiber and spectrum differential integration method," *Optics Communications*, 2014, 313: 270–275.

[17] B. Qi, G. R. Pickrell, J. C. Xu, P. Zhang, Y. H. Duan, W. Peng, *et al.*, "Novel data processing techniques for dispersive white light interferometer," *Optical Engineering*, 2003, 42(11): 3165–3171.

[18] Y. Jiang, "High-resolution interrogation technique for fiber optic extrinsic Fabry-Perot interferometric sensors by the peak-to-peak method," *Applied Optics*, 2008, 47(7): 925–932.

[19] C. J. Qi, M. H. Yang, D. W. Lee, W. J. Xie, and J. X. Dai, "Improved sensitivity of fiber Fabry-Perot interferometer based on phase-tracking algorithm," *IEEE Sensors Journal*, 2015, 15(10): 5834–5838.

[20] X. H. Liu, M. S. Jiang, Q. M. Sui, and F. R. Song, "Temperature sensitivity characteristics of HCPCF-based Fabry-Perot interferometer," *Optics Communications*, 2016, 359: 322–328.

[21] M. S. Jiang, Q. M. Sui, Z. W. Jin, F. Y. Zhang, and L. Jia, "Temperature-independent optical fiber Fabry-Perot refractive-index sensor based on hollow-core photonic crystal fiber," *Optik – International Journal for Light and Electorn Optics*, 2014, 125(13): 3295–3298.

[22] A. Savitzky and M. J. E. Golay, "Smoothing and differentiation of data by simplified least squares procedures," *Analytical Chemistry*, 1964, 36(8): 1627–1639.